Polymer 52 (2011) 2792–2798

Contents lists available at ScienceDirect

Polymer

journal homepage: www.elsevier.com/locate/polymer

A crystalline low-bandgap polymer comprising dithienosilole and thieno[3,4-*c*]pyrrole-4,6-dione units for bulk heterojunction solar cells

Mao-Chuan Yuan, Yi-Jen Chou, Chia-Min Chen, Chang-Lung Hsu, Kung-Hwa Wei*

Department of Materials Science and Engineering, National Chiao Tung University, 300 Hsinchu, Taiwan

ARTICLE INFO

Article history:
Received 30 January 2011
Received in revised form
20 April 2011
Accepted 26 April 2011
Available online 5 May 2011

Keywords:
Crystalline conjugated polymer
Thieno[3,4-c]pyrrole-4,6-dione
Polymer solar cells

ABSTRACT

We have used Stille coupling polymerization to synthesize a new low-bandgap conjugated polymer, **PDTSTPD**, that consists of an electron-rich dithieno[3,2-*b*:2′,3′-*d*]-silole (DTS) unit and an electron-deficient thieno[3,4-*c*]pyrrole-4,6-dione (TPD) moiety. The polymer exhibited an excellent thermal stability, crystalline characteristics, a broad spectral absorption, and a deep highest occupied molecular orbital (HOMO) energy level, resulting from combination of the rigid TPD and the coplanar DTS units in the polymer backbone. Moreover, the presence of the silicon atoms along the polymer chain ensured **PDTSTPD** having strong interchain stacking and good hole mobility. An optimal device incorporating the **PDTSTPD**:$PC_{71}BM$ blend at a weight ratio of 1:1 provided a power conversion efficiency of 3.42%.

1. Introduction

Interest in polymer solar cells (PSCs), which exhibit flexibility and solution-processability, has advanced dramatically because of their fascinating potential for low-cost, large-area production [1,2,3]. PSCs featuring bulk heterojunctions (BHJ) configurations, where the photoactive layers ordinarily consist of electron-donating polymers and electron-accepting fullerene derivatives, have been investigated extensively in recent years [4,5,6,7]. Many studies of PSCs have focused on the development of donor–acceptor (D–A) conjugated polymers because of their tunable optical/electronic properties and ambipolar charge transporting properties [8,9,10,11,12,13,14,15]. Specifically, the D–A design is a powerful strategy for narrowing the optical bandgap of polymers and thereby allowing greater harvesting of photons. Several low-bandgap D–A polymers have promising potential for use in PSC applications. For example, polymers containing rigid electron-donating carbazole [16,17,18,19,20], benzo[1,2-*b*:4,5-*b*′]dithiophene (BDT) [21,22,23,24,25], and dithieno[3,2-*b*:2′,3′-*d*]silole (DTS) [26,27,28,29] moieties, when conjugated with various electron-withdrawing units, can provide power conversion efficiencies (PCEs) of up to 7% after systematic optimization.

Several features are necessary when designing an efficient low-bandgap polymer: a narrow bandgap for enhanced photon harvesting; a low-lying highest occupied molecular orbital (HOMO) energy level to ensure high open-circuit voltages (V_{oc}); sufficient lowest occupied molecular orbital (LUMO) offsets for efficient charge dissociation; and crystalline characteristics to ensure good charge transport. Therefore, the selection of suitable electron acceptors and donors must be made by considering their intrinsic properties.

The thieno[3,4-*c*]pyrrole-4,6-dione (TPD) moiety is an attractive material because its rigid, fused, strongly electron-withdrawing structure can increase the thermal stability, enhance the polymeric chain interactions, narrow the optical bandgap, and lower the HOMO energy level when incorporated in a polymeric backbone. Notably, D–A polymers containing TPD moieties have displayed good PCEs of 3–6% when applied in PSCs [30,31,32,33,34]. In addition, we recently reported efficient PSCs based on the D–A polymer **PBTTPD**, which featured the electron-donating bithiophene units and the electron-deficient TPD moieties in its main chain and, therefore, high crystallinity and a low-lying HOMO energy level; these PSCs exhibited good hole mobility, high values of V_{oc}, and, when optimized, an excellent PCE of 4.7% [35].

In this study, we prepared a coplanar, electron-rich DTS donor unit featuring a silicon atom at its bridging 5-position; ordinarily, the presence of the silicon atom in the polymer backbone enhanced the interchain packing and carrier transporting ability of a polymer [27,28,36]. Furthermore, based on the several advantageous properties of the electron-deficient TPD moiety, we prepared a new low-bandgap D–A conjugated polymer **PDTSTPD**, in which the TPD moiety was conjugated with the electron-rich DTS unit to provide crystalline characteristics, a narrow optical bandgap, and a deep HOMO energy level—all desirable properties for application in PSCs.

* Corresponding author. Tel.: +886 35 731871; fax: +886 35 724727.
E-mail address: khwei@mail.nctu.edu.tw (K.-H. Wei).

0032-3861/$ – see front matter © 2011 Elsevier Ltd. All rights reserved.
doi:10.1016/j.polymer.2011.04.057

2. Experimental section

2.1. Materials and synthesis

1,3-Dibromo-5-ethylhexylthieno[3,4-*c*]pyrrole-4,6-dione (**M1**) [35] and 3,3′-dioctylsilylene-2,2′-bithiophene [36,37] were prepared according to reported procedures. [6,6]-Phenyl-C_{71}-butyric acid methyl ester ($PC_{71}BM$) was purchased from Nano-C. All other reagents were used as received without further purification, unless stated otherwise.

2.1.1. 4,4′-dioctyl-5,5′-bis(trimethylstannyl)dithieno[3,2-b:2′,3′-d] silole (*M2*)

n-BuLi (2.5 M, 2.8 mL, 7.0 mmol) was added dropwise to a stirred solution of 3,3′-dioctylsilylene-2,2′-bithiophene (1.06 g, 2.53 mmol) in anhydrous THF (20 mL) under N_2 at −78 °C. The mixture was stirred at this temperature for 20 min and then warmed to room temperature for 2 h. After cooling again to −78 °C, trimethylstannyl chloride (1 M in hexane, 7.5 mL, 7.5 mmol) was added and then the mixture was warmed gradually to room temperature and stirred overnight. The mixture was poured into water and extracted with Et_2O (3 × 40 mL). The combined organic layers were washed thrice with water (100 mL), dried ($MgSO_4$), and concentrated under reduced pressure to afford **M2** (1.66 g, 88%) as a yellow liquid. ^{1}H NMR (Fig. S1) (300 MHz, $CDCl_3$), δ (ppm): 7.08 (s, 1H), 1.22–1.44 (m, 24H), 0.84–0.90 (m, 10H), 0.37 (s, 18H). MS (*m*/*z*): $[M]^+$ calcd for $C_{30}H_{54}S_2SiSn_2$, 744.1; found, 744.

2.1.2. Polymer *PDTSTPD*

M1 (110 mg, 0.260 mmol), **M2** (193.5 mg, 0.260 mmol), and tri(*o*-tolyl)phosphine [P(*o*-Tol)$_3$; 6.3 mg, 8.0 mol%] were dissolved in dry chlorobenzene (CB, 3 mL) and deoxygenated with N_2 for 15 min. Tris(dibenzylideneacetone)dipalladium [$Pd_2(dba)_3$; 4.8 mg, 2.0 mol %] was added and the solution was again deoxygenated for 15 min. The reaction mixture was heated at 120 °C for 48 h under N_2 and then 2-tributylstannylthiophene (0.16 mL) and 2-bromothiophene (0.05 mL), the end-capping units, were added individually to the solution, with subsequent heating for 6 h each time. After cooling to room temperature, the solution was added dropwise into MeOH (100 mL). The crude polymer was collected, dissolved in hot CB, filtered through a 0.5-μm poly(tetrafluoroethylene) (PTFE) filter, and reprecipitated in MeOH. The solid was washed with acetone and $CHCl_3$ in a Soxhlet apparatus. The $CHCl_3$ solution was concentrated and then added dropwise into MeOH. Finally, the polymer was collected and dried under vacuum to give **PDTSTPD** (125 mg, 70.5%). ^{1}H NMR (Fig. S2) (500 MHz, $C_2D_2Cl_4$), δ (ppm): 8.01 (s, 2H), 3.67 (br, 2H), 1.99 (br, 1H), 0.94–1.43 (m, 48H). Anal. calcd for $C_{38}H_{53}NO_2S_3Si$: C, 67.11; H, 7.85; N, 2.06; found: C, 67.80; H, 7.93; N, 1.73.

2.2. Measurements and characterization

^{1}H NMR spectra were recorded using a Varian UNITY 500-MHz spectrometer. Thermogravimetric analysis (TGA) was performed using a TA Instruments Q500; the thermal stabilities of the samples were determined under a N_2 atmosphere by measuring their weight losses while heating at a rate of 20 °C min^{-1}. Differential scanning calorimetry (DSC) was performed using a Perkin–Elmer Pyris 1 unit operated at heating and cooling rates of 20 and 40 °C min^{-1}, respectively. Size exclusion chromatography (SEC) was performed using a Waters chromatography unit interfaced with a Waters 1515 differential refractometer; polystyrene was the standard; the temperature of the system was set at 45 °C and THF was the eluant. UV–Vis spectra of dilute DCB solutions (1×10^{-5} M) were recorded at ca. 25 and 55 °C using a Hitachi U-4100 spectrophotometer. Solid film for UV–Vis analysis was obtained by spin-coating the polymer solution onto a quartz substrate. Cyclic voltammetry (CV) of the polymer film was performed using a BAS 100 electrochemical analyzer operated at a scan rate of 50 mV s^{-1}; the solvent was anhydrous MeCN, containing 0.1 M tetrabutylammonium hexafluorophosphate ($TBAPF_6$) as the supporting electrolyte. The potentials were measured against a Ag/Ag^+ (0.01 M $AgNO_3$) reference electrode; ferrocene/ferrocenium ion (Fc/Fc^+) was used as the internal standard (0.09 V). The onset potentials were determined from the intersection of two tangents drawn at the rising and background currents of the cyclic voltammogram. HOMO and LUMO energy levels were estimated relative to the energy level of the ferrocene reference (4.8 eV below vacuum level) [21,38]. The X-ray diffraction pattern of the pristine polymer thin film was measured using a Bruker D8 high-resolution X-ray diffractometer operated in grazing-incidence mode. Topographic and phase images of the polymer:PCBM films (surface area: 5×5 μm^2) were obtained using a Digital Nanoscope III atomic force microscope operated in the tapping mode under ambient conditions. The thickness of the active layer of device was measured using a Veeco Dektak 150 surface profiler. Transmission electron microscopy (TEM) images of the copolymer:$PC_{71}BM$ films were recorded using a FEI T12 TEM operating at 120 keV.

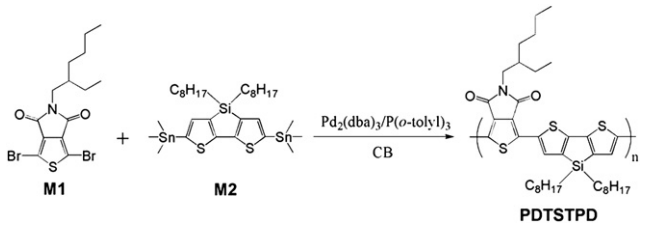

Scheme 1. Synthetic Route and Structure of Polymer **PDTSTPD**.

2.3. Fabrication and characterization of photovoltaic devices

Indium tin oxide (ITO)-coated glass substrates were cleaned stepwise in detergent, water, acetone, and isopropyl alcohol (ultrasonication; 20 min each) and then dried in an oven for 1 h; subsequently, the substrates were treated with UV ozone for 30 min prior to use. A thin layer (ca. 20 nm) of poly(ethylenedioxythiophene):poly(styrene sulfonate) (PEDOT:PSS, Baytron P VP AI 4083) was spin-coated (5000 rpm) onto the ITO substrates. After baking at 140 °C for 20 min in air, the substrates were

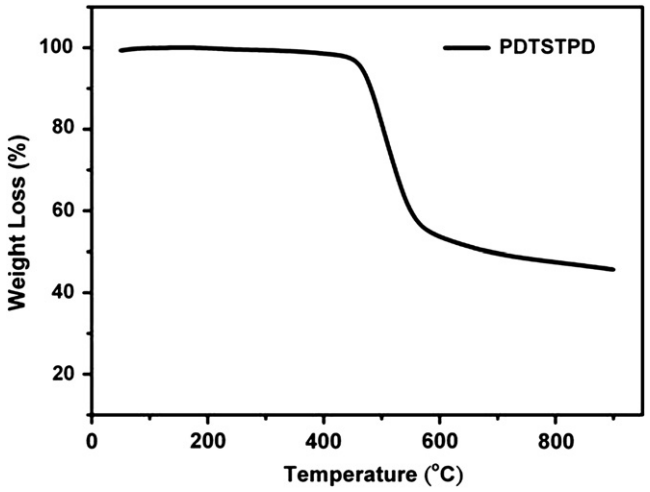

Fig. 1. TGA thermogram of the polymer **PDTSTPD**, recorded at a heating rate of 20 °C min^{-1} under a N_2 atmosphere.

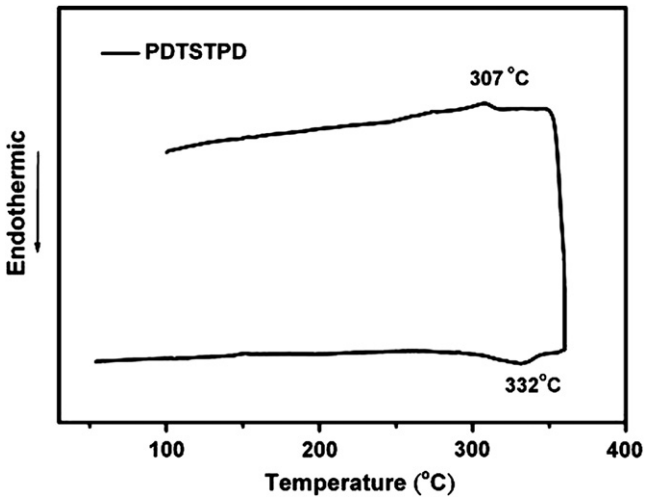

Fig. 2. DSC trace of the polymer **PDTSTPD**, recorded at a heating rate of 20 °C min^{-1} and a cooling rate of 40 °C min^{-1} under a N_2 atmosphere.

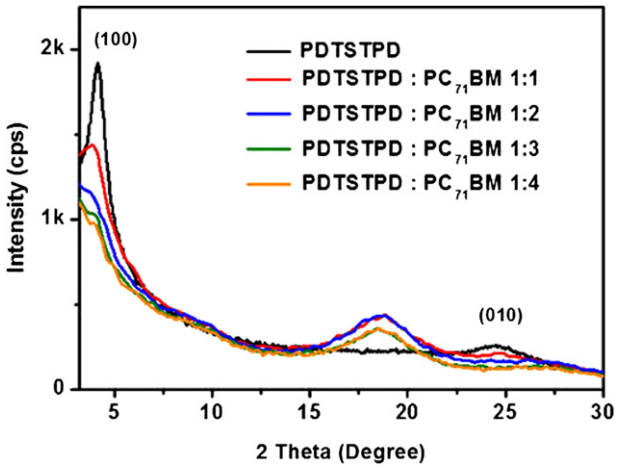

Fig. 3. X-ray diffraction pattern of the pristine **PDTSTPD** film and **PDTSTPD**:$PC_{71}BM$ blends at various weight ratios (w/w).

transferred to a N_2-filled glovebox. The polymer and $PC_{71}BM$ were co-dissolved in dichlorobenzene (DCB) at various weight ratios, but with a fixed total concentration (30 mg mL^{-1}). The blend solution was stirred continuously for 12 h at 60 °C, filtered through a PTFE filter (0.2 μm), the photoactive layer was obtained by spin coating the blend solution onto the ITO/PEDOT:PSS surface at 800 rpm for 60 s with further special treatment for 20 min at 90 °C. The thicknesses of the photoactive layers were ca. 85–95 nm. Finally, an Al (100 nm) layer was thermally evaporated through a shadow mask under a vacuum of less than 1×10^{-6} torr. The effective layer area of one cell was 0.04 cm^2. The current density–voltage (J–V) characteristics were measured using a Keithley 2400 source-meter. The photocurrent was measured under simulated AM 1.5 G illumination at 100 mW cm^{-2} using a Xe lamp–based Newport 66902 150 W solar simulator. A calibrated silicon photodiode with a KG-5 filter was employed to check the illumination intensity. External quantum efficiency (EQE) was measured using an SRF50 system (Optosolar, Germany). A calibrated mono-silicon diode exhibiting a response at 300–900 nm was used as a reference. For hole mobility measurements, the hole only devices were fabricated with structures of ITO/PEDOT:PSS/polymer/Au and ITO/PEDOT:PSS/polymer:$PC_{71}BM$/Au. The hole mobility was determined by fitting the dark J–V curve into the space-charge-limited current (SCLC) method [11,39], based on the equation

$$J = \frac{9}{8}\varepsilon_0\varepsilon_r\mu_h\frac{V^2}{L^3}$$

where ε_0 is the permittivity of free space, ε_r is the dielectric constant of the material, μ_h is the hole mobility, V is the voltage drop across the device, and L is the thickness of active layer.

3. Results and discussion

3.1. Synthesis and characterization of the polymer

Scheme 1 displays the synthetic routes that we used to prepare the monomers and the polymer. The **TPD**-based polymer **PDTSTPD** was prepared through Stille polymerization using the corresponding monomers **M1**/**M2** and $Pd_2(dba)_3$/P(*o*-Tol)$_3$ as the catalyst; the polymer comprised the DTS and TPD units. **PDTSTPD** had a number-average molecular weight (M_n) of 12 kg mol^{-1}, with a polydispersity of 2.0, as determined through gel permeation chromatography (GPC) using polystyrene standards. The polymer was readily soluble in THF, $CHCl_3$, CB, and DCB. We investigated the thermal behavior of the polymer through TGA and DSC analyses. The TGA curve (Fig. 1) revealed that the polymer exhibited an excellent thermal stability, with 5%-weight-loss temperatures (T_d) greater than 450 °C. Fig. 2 displays the thermal transition of the polymer in DSC analysis; Table 1 summarizes the related data. In the endothermic trace, **PDTSTPD** exhibited a melting point at 332 °C, but glass transition was not detectable. In contrast to the exothermic trace, the polymer exhibited a distinct crystallization point at 307 °C. Table 1 summarizes the molecular weight, polydispersity, and thermal properties of the polymer. We confirmed the crystalline characteristic from the grazing-incidence X-ray diffraction pattern of the polymer thin film (Fig. 3). **PDTSTPD** exhibited sharp diffraction peaks at 4.1° which we assign to its (100) crystal plane; the *d*-spacing of 21.5 Å correspond to the interchain separation defined by its alkyl side chains. In addition,

Table 1
Molecular weights and thermal properties of the polymers.

Polymer	M_n (10^4)	PDI	T_c (°C)	T_m (°C)	T_d (°C)
PDTSTPD	1.2	2.0	307	332	465

Glass transition temperature was not detectable.

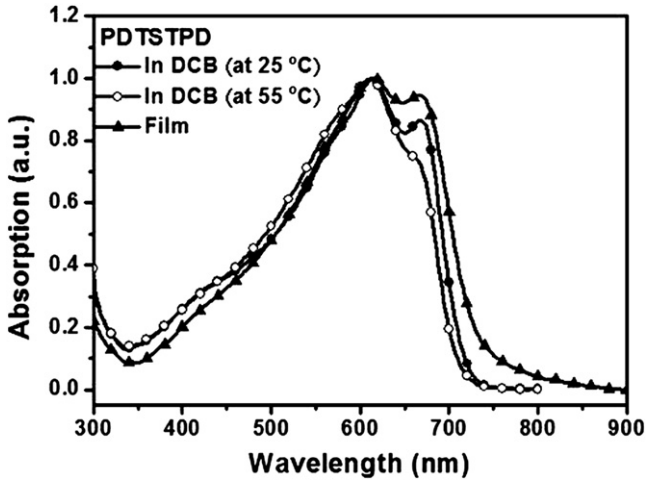

Fig. 4. UV–Vis absorption spectra of **PDTSTPD** in dilute DCB (1×10^{-5} M) solutions, recorded individually at 25 and 55 °C, and as solid film.

Table 2
Optical and Redox Properties of the Polymers.

	Absorption, λ_{max} (nm)		E_g^{opt} (eV)[a]	E_{onset}^{ox} (V)	E_{onset}^{red} (V)	HOMO (eV)[b]	LUMO (eV)[b]
	Solution	Film					
PDTSTPD	611,665	614,667	1.70	0.66	−1.65	−5.46	−3.15

[a] Estimated from the onset wavelength absorptions of the solid films.
[b] Calculated from the corresponding onset potentials.

we assign the broad reflection appearing at 24.5° to its (010) crystal plane, corresponding to a short distance of 3.6 Å, which arose from the facial π–π stacking of the polymeric chains. The crystalline characteristic of the polymer appeared favorable for charge transport within PSCs.

3.2. Photophysical properties

Fig. 4 presents absorption spectra of the polymer, recorded in dilute DCB solutions and as solid film; the spectra of the solutions were recorded at both ca. 25 and 55 °C. Table 2 summarizes the spectral data. In solution at 25 °C, **PDTSTPD** exhibited the absorption maximum at 611 nm, which we assign to the internal charge transfer (ICT) interaction between the electron-accepting **TPD** and electron-donating **DTS** units. Moreover, a significant vibronic shoulder appeared at 665 nm while the shoulder diminished when we heated the solutions at 55 °C, implying that a certain degree of π–π aggregation was already in effect in the solution states [28]. The absorption spectra of the polymer in the solid state was similar to their corresponding solution spectra, with only slight red-shifts of 3 nm of their absorption maxima, meaning some intermolecular interactions were already existent in its solution [31]. Moreover, the intensity of the vibronic shoulder of the polymer in the solid state was increased significantly relative to that in solution, indicating that much stronger interchain π–π stacking occurred in the solid state. The optical bandgap (E_g^{opt}) of **PDTSTPD**, estimated from the onset of the absorption in its solid film, was 1.70 eV; the value is smaller than that of the polymer **PBTTPD** (1.82 eV) because the presence of the more coplanar and electron-rich **DTS** donor unit in the main chain extended the range of spectral absorption.

3.3. Electrochemical properties

We used CV to investigate the redox behavior of the polymer and obtain its HOMO and LUMO energy levels. Fig. 5 presents the electrochemical behavior of the polymer as a solid film. The polymer exhibited partially reversible oxidative and reductive behavior. **PDTSTPD** had an oxidative onset potential of 0.66 V, arising essentially from oxidation of the electron-donating **DTS** unit. In the reduction trace, the polymer had a reductive onset potential of −1.65 V, which we attributed to the reduction of the electron-deficient **TPD** moiety. On the basis of the onset potentials, we estimated the HOMO and LUMO energy levels relative to the energy level of the ferrocene reference (−4.8 eV below vacuum level). Accordingly, the HOMO and LUMO energy levels of **PDTSTPD** were −5.46 and −3.15 eV, respectively. This deep HOMO energy level was due to the presence of the strongly electron-withdrawing **TPD** moiety in its polymer backbone; moreover, the value (−5.46 eV) was lower than −5.2 eV, suggesting its good stability against oxidization in air [16,40]. The LUMO energy level of **PDTSTPD** was greater than that of $PC_{71}BM$ (−4.2 eV) [41]; thus, a sufficient LUMO offset existed for efficient charge dissociation in the active layer [4,41]. The electrochemical bandgap of the polymer, estimated from the difference between its onset potential for oxidation and reduction, was −2.31 eV; the value is somewhat larger than its optical bandgap (1.70 eV). Such similar difference between the electrochemical and optical bandgap has been observed in studies of other D–A polymers [26,31,42], presumably resulting from the interface barrier for charge injection [42,43].

Table 3
Photovoltaic properties of polymer solar cells incorporating **PDTSTPD**:$PC_{71}BM$ Blends prepared at various weight ratios.

Ratio (w/w)	Thickness (nm)	V_{oc} (V)	J_{sc} (mA cm^{-2})	FF (%)	PCE (%)	R_s (Ω cm^2)	R_{sh} (Ω cm^2)
1:1	97	0.87	4.51	49.4	1.94	55	711
1:1[a]	95	0.86	7.72	51.5	3.42	25	792
1:2	92	0.88	5.34	54.9	2.58	37	724
1:2[a]	94	0.85	6.78	58.8	3.39	27	1180
1:3	90	0.88	5.74	58.7	2.96	22	827
1:3[a]	90	0.85	6.60	59.9	3.36	19	1014
1:4	87	0.87	5.25	59.0	2.69	26	923

[a] Processed with 4 vol% DIO.

3.4. Photovoltaic properties

We investigated the photovoltaic properties of **PDTSTPD** in PSCs having the device structure ITO/PEDOT:PSS/polymer:$PC_{71}BM$/Al, where the active layers were spin-coated from blended DCB solutions. Devices prepared from the polymers and $PC_{71}BM$ at various

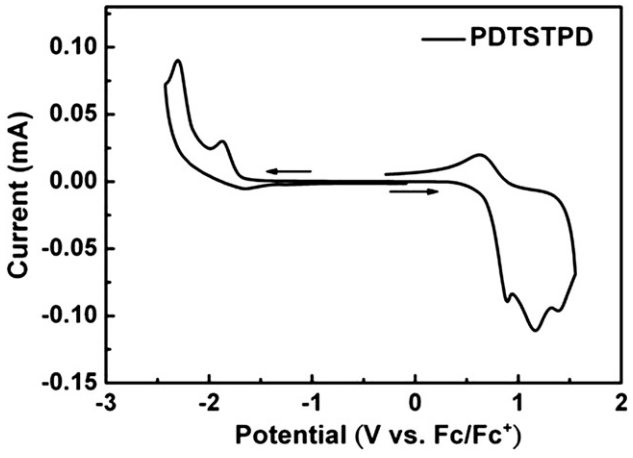

Fig. 5. Cyclic voltammogram of the polymer **PDTSTPD** as solid film.

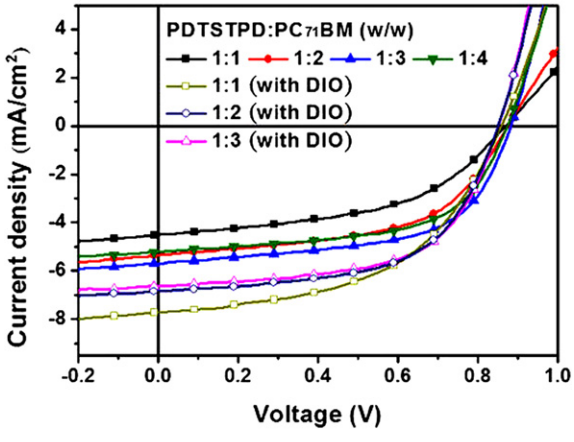

Fig. 6. *J–V* characteristics of PSCs incorporating **PDTSTPD**:$PC_{71}BM$ blends at various weight ratios (w/w).

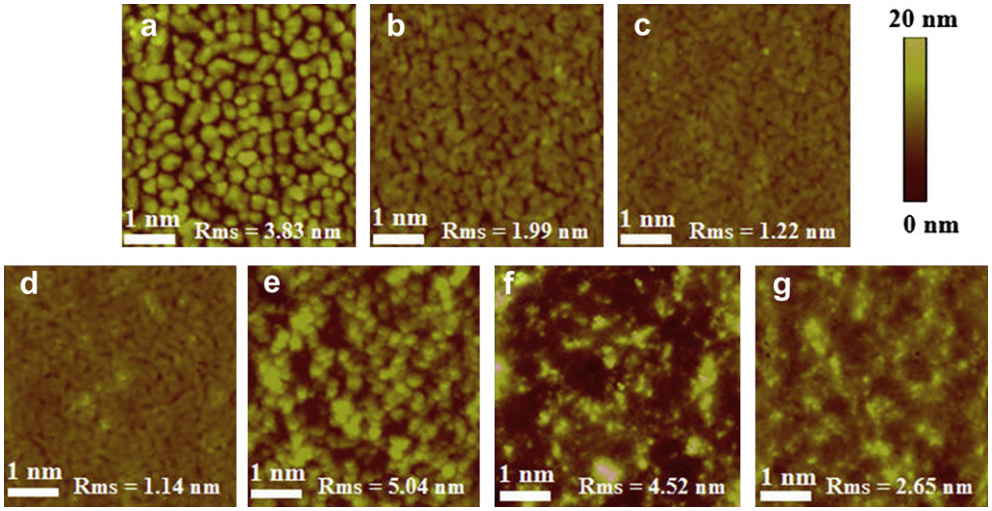

Fig. 7. Topograhic images of **PDTSTPD**:$PC_{71}BM$ blends at weight ratios of (a) 1:1, (b) 1:2, (c) 1:3, (d) 1:4, (e) 1:1 (processed with 4 vol% DIO), (f) 1:2 (processed with 4 vol% DIO) and (g) 1:3 (processed with 4 vol% DIO).

weight ratios were systematically investigated; in some cases, we added a small amount of 1,8-diiodooctane (DIO; 4%, by volume relative to DCB) to optimize the morphologies of the blends. Fig. 6 presents the *J*–*V* curves of the devices incorporating various polymer:$PC_{71}BM$ blend ratios; the values of series resistance (R_s) and shunt resistance (R_{sh}) of devices were estimated according to the equations described in the literature [44]; Table 3 summarizes the corresponding values of V_{oc} and short-circuit current densities (J_{sc}), fill factors (FFs), PCEs, R_s, and R_{sh}. The devices incorporating the **PDTSTPD**:$PC_{71}BM$ blends at various weight ratio exhibited values of V_{oc} of 0.87–0.88 V, related to the difference between the HOMO energy level of the polymer and the LUMO energy level of $PC_{71}BM$ [45]. A device incorporating the **PDTSTPD**:$PC_{71}BM$ blend at a weight ratio of 1:1 exhibited a PCE of 1.94%, with values of V_{oc}, J_{sc}, and FF of 0.87 V, 4.51 mA cm^{-2}, and 49.4%, respectively. When we increased the amount of $PC_{71}BM$ to a weight ratio of 1:3 (w/w), the values of J_{sc}, FF, and PCE of the device improved to 5.74 mA cm^{-2}, 58.7%, and 2.96%, respectively, because of the relatively smaller R_s and larger R_{sh}. The values of J_{sc} and PCE decreased slightly to 5.25 mA cm^{-2} and 2.69%, respectively, upon increasing the amount of $PC_{71}BM$ further to a weight ratio of 1:4. Fig. 7 and Fig. S3 (see Supporting information) display the corresponding topographic and phase images of the **PDTSTPD**:$PC_{71}BM$ blends. We observed a relatively smoother surface with smaller phase-separated domains for the blend at a weight ratio of 1:3, relative to those obtained at weight ratios of 1:1 and 1:2; as a result, better device performance was obtained for the former. Furthermore, when we incorporated DIO (4 vol%) into the 1:3 (w/w) **PDTSTPD**:$PC_{71}BM$ blend, the device exhibited slightly increased values of J_{sc} and FF of 6.60 mA cm^{-2} and 59.9%, respectively, resulting in an increased PCE

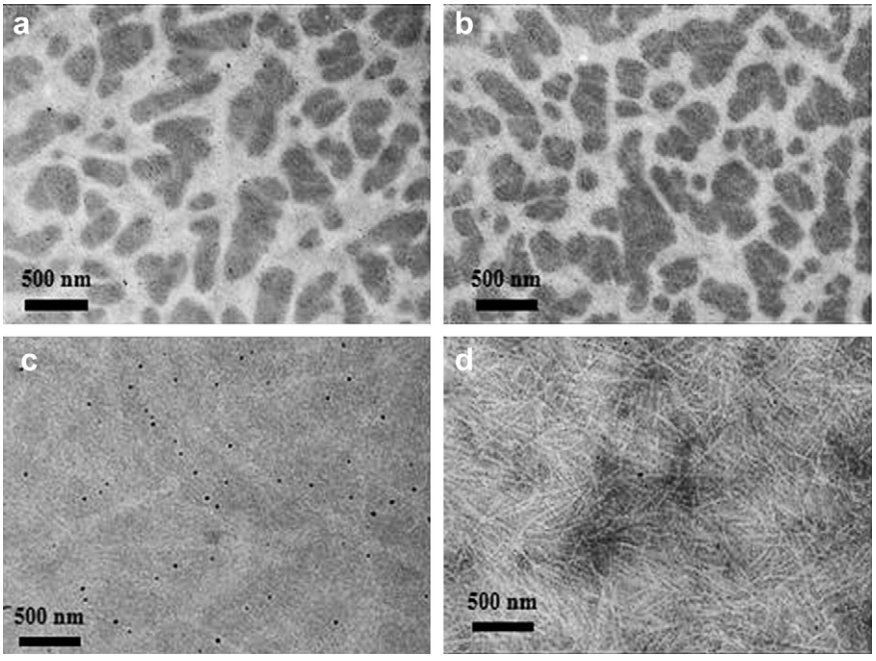

Fig. 8. TEM image of **PDTSTPD**:$PC_{71}BM$ blends at weight ratios of (a) 1:1, (b) 1:3, (c) 1:1 (processed with 4 vol% DIO) and (d) 1:3 (processed with 4 vol% DIO).

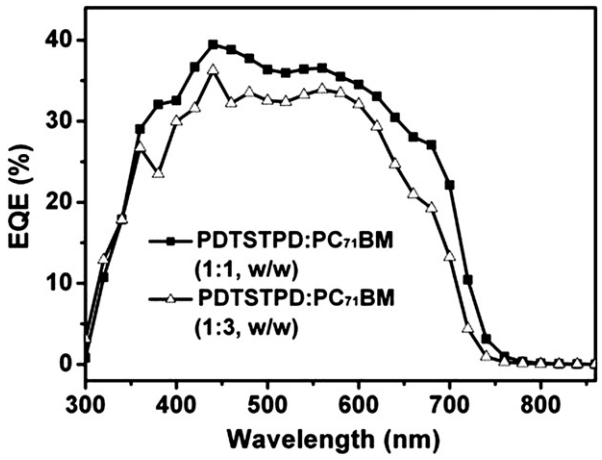

Fig. 9. EQE curves of PSCs incorporating the **PDTSTPD**:$PC_{71}BM$ blends at weight ratios of 1:1 and 1:3 (w/w) (both processed with 4 vol% DIO).

of 3.36%. In addition, the incorporation of 4% DIO (v/v) into the 1:1 (w/w) **PDTSTPD**:$PC_{71}BM$ blend increased the value of J_{sc} significantly to 7.72 mA cm^{-2}, increased the FF slightly to 51.5%, and therefore enhanced the PCE to 3.42%, presumably because more-intimate mixing of **PDTSTPD** and $PC_{71}BM$ resulted in a lower R_s. Fig. 8 shows the TEM images of **PDTSTPD**/$PC_{71}BM$ blend films. Because the electron scattering density of $PC_{71}BM$ is higher than that of the conjugated polymer, the **PDTSTPD** domains appear as bright regions whereas the dark regions can attributed to $PC_{71}BM$ domains. Fig. 8a and b exhibits of the island shape features of aggregated $PC_{71}BM$ domains (dark areas) in the blend films with **PDTSTPD**/$PC_{71}BM$ weight ratios of 1:1 and 1:3, respectively that were processed without additives. In contrast, Fig. 8c and d displays homogeneous morphology for the **PDTSTPD**/$PC_{71}BM$ blend films at weight ratios of the 1:1 and 1:3 that were processed with 4 vol% DIO additive, indicating that the incorporation of 4% DIO (v/v) optimized the miscibility of polymer chains with $PC_{71}BM$. Through optimization of the blend morphology, such high values of J_{sc} and PCE were also possible for the **PDTSTPD**:$PC_{71}BM$ blend at a weight ratio of 1:1. Fig. 9 presents the EQE curves of the optimized devices based on the **PDTSTPD**:$PC_{71}BM$ blends at weight ratios of the 1:1 and 1:3 (w/w) (both processed with 4 vol% DIO). These devices exhibited broad EQE responses from 300 to 750 nm, which we attribute to the enlarged spectral absorptions of the polymer. The

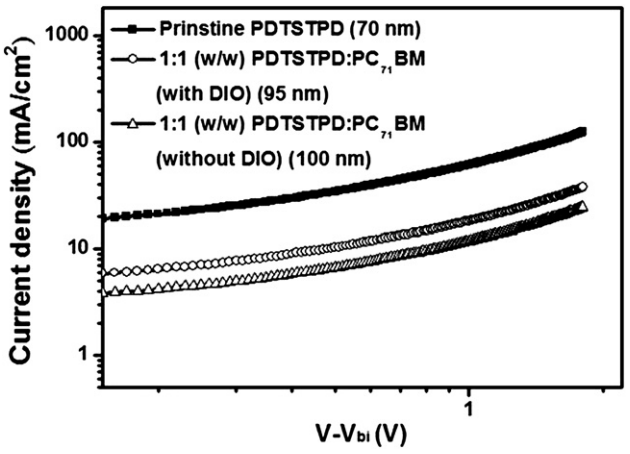

Fig. 10. Dark J–V curves for hole-dominated carrier devices incorporating the pristine **PDTSTPD** film, the 1:1 (w/w) **PDTSTPD**:$PC_{71}BM$ blend and the 1:1 (w/w) **PDTSTPD**:$PC_{71}BM$ blend (processed with 4 vol% DIO).

device of the 1:1 (w/w) **PDTSTPD**:$PC_{71}BM$ blend exhibited a higher EQE response than that of the 1:3 (w/w) **PDTSTPD**:$PC_{71}BM$ blend, with a maximum of 40% at 440 nm, consistent with its higher value of J_{sc}. The relatively higher EQE responses between 400 and 550 nm for these devices were caused by the significant absorption of $PC_{71}BM$ in this short wavelength range. Moreover, the values of J_{sc} calculated by integrating the EQE curves are rather close to those obtained from the J–V measurements with a discrepancy smaller than 3%. In addition, hole mobility of a conjugated polymer is an important factor influencing its applicability in PSCs. Fig. 10 displays the hole-dominated curves of the devices based on **PDTSTPD**. The hole mobilities of the pristine **PDTSTPD**, the 1:1 (w/w) **PDTSTPD**:$PC_{71}BM$ and the 1:1 (w/w) **PDTSTPD**:$PC_{71}BM$ (processed with 4 vol% DIO) were 8.3×10^{-5}, 5.4×10^{-5} and 6.2×10^{-5} cm^2 V^{-1} s^{-1}, respectively; these decent value resulted from its intrinsic crystalline property, which can promote charge transport in the devices.

4. Conclusions

We prepared a new low-bandgap polymer, **PDTSTPD**, by conjugating an electron-deficient thieno[3,4-*c*]pyrrole-4,6-dione (TPD) moiety with an electron-rich dithieno[3,2-*b*:2′,3′-*d*]silole (DTS) unit. Because of the presence of TPD moieties, the polymer exhibited an excellent thermal stability, crystalline characteristics, a broad spectral absorption, and a low-lying HOMO energy level—all features that are desirable for solar cell applications. Manipulating the compositions and modulating the morphologies of the blends allowed us to optimize devices based on these polymer:$PC_{71}BM$ blends. An optimal device incorporating the **PDTSTPD**:$PC_{71}BM$ blend at a weight ratio of 1:1 displayed a better PCE of 3.42%.

Acknowledgment

We thank the National Science Council, Taiwan, for financial support (NSC 98-2120-M-009-006).

Appendix. Supplementary data

Supplementary data related to this article can be found online at doi:10.1016/j.polymer.2011.04.057.

References

[1] Yu G, Gao J, Hummelen JC, Wudl F, Heeger AJ. Science 1995;270:1789–91.
[2] Günes S, Neugebauer H, Sariciftci NS. Chem Rev 2007;107:1324–38.
[3] Krebs FC, Jorgensen M, Norrman K, Hagemann O, Alstrup J, Nielsen TD, et al. Sol Energy Mater Sol Cells 2009;93:422–41.
[4] Thompson BC, Fréchet JMJ. Angew Chem Int Ed 2008;47:58–77.
[5] Li G, Shrotriya V, Huang J, Yao Y, Moriarty T, Emery K, et al. Nat Mater 2005;4:864–8.
[6] Li YF, Zou YP. Adv Mater 2008;20:2952–8.
[7] Chiu M-Y, Jeng U-S, Su C-H, Liang K-S, Wei K-H. Adv Mater 2008;20:2573–8.
[8] Chang Y-T, Hsu S-L, Chen G-Y, Su M-H, Singh T-A, Diau EW-G, et al. Adv Funct Mater 2008;18:2356–65.
[9] Huang F, Chen KS, Yip HL, Hau SK, Acton O, Zhang Y, et al. Am Chem Soc 2009;131:13886–7.
[10] Zoombelt AP, Leenen MAM, Fonrodona M, Nicolas Y, Wienk MM, Janssen RAJ. Polymer 2009;50:4546–70.
[11] Chang Y-T, Hsu S-L, Su M-H, Wei K-H. Adv Mater 2009;21:2093–7.
[12] Zhou E, Cong J, Tajima K, Hashimoto K. Chem Mater 2010;22:4890–5.
[13] Li Y, Li H, Xu B, Li Z, Chen F, Feng D, et al. Polymer 2010;51:1786–95.
[14] Inganäs O, Zhang F, Tvingstedt K, Andersson LM, Hellström S, Andersson MR. Adv Mater 2010;22:E100–16.
[15] Zhao W, Cai W, Xu R, Yang W, Gong X, Wu H, et al. Polymer 2010;51:3196–202.
[16] Blouin N, Michaud A, Gendron D, Wakim S, Blair E, Neagu-Plesu R, et al. J Am Chem Soc 2008;130:732–42.
[17] Park SH, Roy A, Beaupré S, Cho S, Coates N, Moon JS, et al. Nat Photonics 2009;3:297–302.

[18] Qin R, Li W, Li C, Du C, Veit C, Schleiermacher HF, et al. J Am Chem Soc 2009; 131:14612–3.
[19] Chen G-Y, Lan S-C, Lin P-Y, Chu C-W, Wei K-H. J Polym Sci Part A Polym Chem 2010;48:4456–64.
[20] Hsu S-L, Chen C-M, Wei K-H. J Polym Sci Part A Polym Chem 2010;48: 5126–34.
[21] Liang Y, Feng D, Wu Y, Tsai S-T, Li G, Ray C, et al. J Am Chem Soc 2009;131: 7792–9.
[22] Chen H-Y, Hou J, Zhang S, Liang Y, Yang G, Yang Y, et al. Nat Photonics 2009;3: 649–53.
[23] Zhou H, Yang L, Price SC, Knight KJ, You W. Angew Chem Int Ed 2010;49:7992–5.
[24] Yuan M-C, Chiu M-Y, Chiang C-M, Wei K-H. Macromolecules 2010;43: 6270–7.
[25] Zhang G, Fu Y, Xie Z, Zhang Q. Polymer 2011;52:415–21.
[26] Hou J, Chen H-Y, Zhang S, Li G, Yang Y. J Am Chem Soc 2008;130:16144–5.
[27] Scharber MC, Koppe M, Gao J, Cordella F, Loi MA, Denk P, et al. Adv Mater 2010;22:367–70.
[28] Chen H-Y, Hou J, Hayden AE, Yang H, Houk KN, Yang Y. Adv Mater 2010;22:371–5.
[29] Hoven CV, Dang XD, Coffin RC, Peet J, Nguyen T-Q, Bazan GC. Adv Mater 2010; 22:E63–6.
[30] Zou Y, Najari A, Berrouard P, Beaupré S, Aïch BR, Tao Y, et al. J Am Chem Soc 2010;132:5330–1.
[31] Zhang Y, Hau SK, Yip H-L, Sun Y, Acton O, Jen AK-Y. Chem Mater 2010;22: 2696–8.
[32] Piliego C, Holcombe TW, Douglas JD, Woo CH, Beaujuge PM, Fréchet JMJ. J Am Chem Soc 2010;132:7595–7.
[33] Zhang G, Fu Y, Zhang Q, Xie Z. Chem Commun 2010;46:4997–9.
[34] Guo X, Xin H, Kim FS, Liyanage ADT, Jenekhe SA, Watson MD. Macromolecules 2011;44:269–77.
[35] Yuan M-C, Chiu M-Y, Liu S-P, Chen C-M, Wei K-H. Macromolecules 2010;43: 6936–8.
[36] Lu G, Usta H, Risko C, Wang L, Facchetti A, Ratner MA, et al. J Am Chem Soc 2008;130:7670–85.
[37] Welch GC, Coffin R, Peet J, Bazan GC. J Am Chem Soc 2009;131:10802–3.
[38] Pommerehne J, Vestweber H, Guss W, Mahrt RF, Bässler H, Porsch M, et al. Adv Mater 1995;7:551–4.
[39] Melzer C, Koop EJ, Mihailetchi VD, Blom PWM. Adv Funct Mater 2004;14: 865–70.
[40] de Leeuw DM, Simenon MMJ, Brown AR, Einerhand REF. Synth Met 1997;87: 53–9.
[41] Lindgren LJ, Zhang F, Andersson M, Barrau S, Hellström S, Mammo W, et al. Chem Mater 2009;21:3491–502.
[42] Wu P-T, Kim FS, Champion RD, Jenekhe SA. Macromolecules 2008;41:7021–8.
[43] Chen Z-K, Huang W, Wang L-H, Kang E-T, Chen BJ, Lee CS, et al. Macromolecules 2000;33:9015–25.
[44] Moliton A, Nunzi J-M. Polym Int 2006;55:583–600.
[45] Scharber MC, Mühlbacher D, Koppe M, Denk P, Waldauf C, Heeger AJ, et al. Adv Mater 2006;18:789–94.